Journal of New Technology and Materials (JNTM)
J. New Technol. Mater.
Vol. 10, N°01 (2020)82-89

OEB Univ. Publish. Co.

Effect of annealing temperature of bismuth ferrite on morphology, magnetic properties and the photocatalytic degradation of sodium salt of 4–dimethylaminoazobenzene–4–sulfonic acid dye

K. Karthikeyan[a] and A. Thirumoorthi[b*]

[a]*Research and Development centre, Bharathiar University, Coimbatore, Tamilnadu, India.*

[b]*Assistant Professor, Post Graduate Department of Chemistry, Government Arts College, Udumalpet – 642 126, Tamilnadu, India.*

* Corresponding author, E-mail address: dramoorthiudt@gmail.com.

Received date: May 06, 2020; accepted date: May 28, 2020

Abstract

Industrial waste water management includes the removal of colour making pigments and dyes from them, which is a tedious task. Green and recyclable methods to remove the pigments are the need of the present. Among various methods, Photocatalytic approach are becoming quite popular now-a-days. This paper reveals the studies on photocatalytic effect of multiferroic bismuth ferrite (BFO) nanoparticles for water treatment. The BFO nanoparticles have been synthesized by sol-gel technique and annealed between 300°C and 700°C and were characterized by FT- IR, XRD, SEM, PL and VSM studies. The photocatalytic activity of BFO has been studied in aqueous solution of Sodium salt of 4 – dimethylaminoazobenzene – 4 – sulfonic acid dye, the well-known Methyl Orange (MO), using various pH of 2, 7 and10 under sun light irradiation. The absorption magnitude is higher for BFO – 400 and the band gap was found to be 1.88 eV. The morphology and surface studies indicates the nano characteristics of the BFO samples. Further the photoluminescence studies revealed the enhanced photocatalytic property of BFO – 400 sample which can effectively be used for waste water management applications.

Keywords: $BiFeO_3$*;* Annealing temperature*;* Luminescence*;* VSM*;* Photodegradation.

1. Introduction

In the recent past, the removal of colouring materials like pigments and dyes from the industrial waste water is a prime concern that attracted many researchers. The increasing concentration of organic pollutants from industries leads detrimental effects to environment including aquatics and human beings. A green and recyclable methodology is vital for the purification and separation of these contaminants. Though several photocatalysts have been used for this purposes, semiconductor based photocatalysts are widespread and useful in simple condition to use natural sun light or artificial UV light irradiation [1]. Semiconductor based photocatalysts like TiO_2, SnO_2 and ZnO have been used as an efficient photocatalyst since they possess excellent photocatalytic activity, high chemical stability, non-toxicity and low cost and absorbs only small amounts of sunlight due to wide band gap [2]. Azo pigments such as Methyl Orange (MO), Rhodamine – B (Rh–B) and Congo Red (CR) are often used dyes in industries, are highly hazardous in environment [3–5]. Therefore, these organic pollutants can be decomposed through photocatalysis using semi conducting metal oxide under UV light irradiation. The availability of UV light in solar spectrum is very low, which leads to the development of new high performance materials that can act as active photocatalysts under Visible light irradiation. These types of materials are highly essential for practical applications of photocatalytic techniques.

Owing to the narrow band gaps, multiferroic materials of Perovskite type oxides with general composition of ABO_3 in which A is a rare earth element and B is transition metal have more attraction for photocatalysis. Among the several multiferroic materials, $BiFeO_3$ (BFO) is only one that exhibits both ferroelectricity and G – type antiferromagnetism (Curie temperature, $T_c \approx 1103$ K, Neel temperature, $T_N \approx 643$ K) [6]. In addition, the small band gap of BFO (< 3.0 eV) has great attention to explore BFO as an efficient visible light photocatalyst. Recently, it is found that $BiFeO_3$ with 2.18 eV band gap had good photochemical stability [7]. Moreover, $BiFeO_3$ is a magnetic semiconductor material which can be easily separated from aqueous organic contaminations. On the other hand, $BiFeO_3$ has low surface area and high ratio recombination of electron / hole pairs. This required the combination of BFO with foreign materials so as to result in a high surface area and improved electron transport ability [8]. Besides potential electronic applications, BFO powders have been used as a novel visible light photocatalyst [9] and a vector in drug targeting to minimize the side effects of drugs in chemotherapy [10]. Li et al.

revealed that BFO synthesized hydrothermally has uniform microcrystals with various morphologies exhibited high visible light photocatalytic activity for the photodegradation of Congo red [11]. Huo et al. prepared BFO mesoporous hollow sphere with high surface area, have high activity in photocatalytic degradation of Rhodamine – B under visible light irradiation [7]. However, the photocatalytic reaction mechanism of pollutant degradation using BFO is still lacking.

In recent research, nanosize effects on the physical properties of both magnetic and ferroelectric counterparts of multiferroic materials have been studied due to their potential applications in various nanoscale devices. It is well known that the photocatalytic activity of photocatalyst is strongly determined by several microstructure factors such as particle size, surface morphology and crystallinity [12]. Among these, the most important are particle size and crystallinity. Small particle size gives rise to large surface area, while crystallinity directly determines the lattice perfection and the defects of the materials. In general, there are two methods to enhance the crystallinity of photocatalyst: (i) prolonging the reaction time and (ii) increasing the reaction temperature. However, both methods will also result in a significant grain growth, which in turn reduces the surface area and may decrease the photocatalytic activity. Thus, a balance between small particle size and high crystallinity is of great importance in preparing photocatalyst. Thus, recently the size dependent photocatalytic properties of BFO nanoparticles have been reported in the open literature.

Sambhu Prasad Pattnaik et al. found that $BiFeO_3$ nanoparticles are synthesized by solid state reaction and annealed at different temperatures. The samples are polycrystalline in nature and absorb maximum fraction of visible light and the sample annealed at 500°C is the best photocatalyst for the de-colorization of Congo red under sun light. This is due to high photocurrent generation, low photoluminescence intensity leads to better charge separation and low recombination rate, high optical absorption, nanorange particle size and better crystallinity [13].

Minglin Jin et al. studied the synthesis of pure phase bismuth ferrite nanoparticles by chemical co-precipitation method by composite precipitants, sintered at 600°C [14]. XRD showed that BFO has R3C crystal symmetry and the particle size was found to be 100 nm to 150 nm. UV – Vis. Diffuse reflectance spectral studies indicates that the band gap energy of BFO is 2.18 eV and it has excellent photocatalytic degradation to methyl orange under visible light.

This research article describes the synthesis and characterization of pure phase bismuth ferrite nanoparticles using ascorbic acid by a sol – gel method and the effects of annealing between 300°C and 700°C have been studied. Also, the effect of photocatalytic activity of BFO nanoparticles have been studied using sodium salt of 4 – dimethylaminoazobenzene – 4 – sulfonic acid dye, commonly known as Methyl Orange (MO) under visible light at different pH values.

2. Experimental Section

2.1. Materials

All the reagents used are obtained from Sigma – Aldrich and Merck, and are used as received without any further purification. Nitric acid of analar grade reagent (A.R) and double distilled water were used for the sample preparation.

2.2. Synthesis of Bismuth Ferrite nanoparticles

Bismuth Ferrite nanoparticles were synthesized using equimolar concentration of bismuth nitrate and iron nitrate dissolved in 40 mL double distilled water with ascorbic acid of 0.005 molar concentration. Then 1.2 mL of nitric acid was added with constant stirring at room temperature for half an hour to form transparent mixture. This solution was heated at 80°C until all the solvents were evaporated. The brown powder obtained was annealed at different temperatures of 300°C – 700°C for two hours. The annealed BFO powders were used as photocatalysts and the samples were designated as BFO–300, BFO–350, BFO–400, BFO–450, BFO–500, BFO–550, BFO–600, BFO–650 and BFO–700.

2.3. Characterization of Bismuth ferrite

UV–Visible absorption spectra were recorded using Shimadzu UV-Visible spectrometer (UV1800, Japan). FT – IR analyses were carried out on a Shimadzu FT – IR spectrometer of Prestige – IR 21 using KBr pellet for the sample preparation. X- ray diffraction studies were performed using an instrument, XRD Shimadzu labX6000 to study the crystalline nature of BFO nanoparticles. The size and morphology of the samples were examined using Scanning electron microscope, SEM Jeol JSM6390. Horiba Jobin Yvon Flurolog–3 Fluorescence spectrophotometer was used to carry out the photoluminescence emission spectra of BFO samples. A commercial HH–15 model vibrating sample magnetometer (VSM, Lakeshore 7410) was used at room temperature to characterize the magnetic properties of $BiFeO_3$ nanoparticles.

2.4. Photocatalytic experiments

Photocatalytic activity of the $BiFeO_3$ was evaluated by measuring the degradation of methyl orange dye under direct sun light irradiation. For this purpose, several glass vessels containing 100ml of the dye solutions ($0.015 mgL^{-1}$) and appropriate quantity of photocatalyst were magnetically stirred in dark for an hour to attain adsorption–desorption equilibrium between the dye and the photocatalyst in solution. Different amounts of photocatalyst ($0.1 – 0.5\ gL^{-1}$) were used for the degradation of 100 mL of methyl orange solution. About 5 mL of the samples were withdrawn from mixture using a micropipette with time intervals of 30, 60, 90, 120 minutes and centrifuged at 5000 rpm for 5 minutes. After

centrifuged, the supernatants were analyzed for the determination of the final concentrations of the dye. The removal of methyl orange from the solution was determined using a UV- Visible spectrophotometer at 464 nm. All the experiments have been carried out at pH of 2, 7 and 10 in order to evaluate the role of pH on photocatalytic activity of BFO nanoparticles.

3. Results and discussion

3. 1. UV– Visible spectral analysis

The UV – Visible absorption spectra of bismuth ferrite nanoparticles at different annealing temperatures displayed the amorphous phase with less steep absorption edge in its absorption spectrum between 500 and 600 nm. This is due to the different electronic environments around the Fe^{3+} and Bi^{3+} cations and other factors such as amorphous phase, the smaller BFO nanostructures, higher lattice strain including the presence of secondary phases. When the temperature increases, the amount of nitrates decreases and the size of BFO nanoparticles increases while the lattice strain decreases which make the absorption edge steeper [15].

Fig. 1(a) illustrates UV – Visible absorption spectra of synthesized BFO nanoparticles annealed at different temperatures of 300°C to 700°C. The BFO samples absorb visible light in the range between 400 and 800 nm and the magnitude of absorbance indicates that the BFO nanoparticles are very active under direct sun light. When the temperature increases, the absorption edge become steeper between 450 and 700nm due to decreased lattice strain and hence the size is increased. BFO – 400 has highest absorbance indicating this sample was highly active under solar radiation and further increasing temperature decrease the absorbance magnitude.

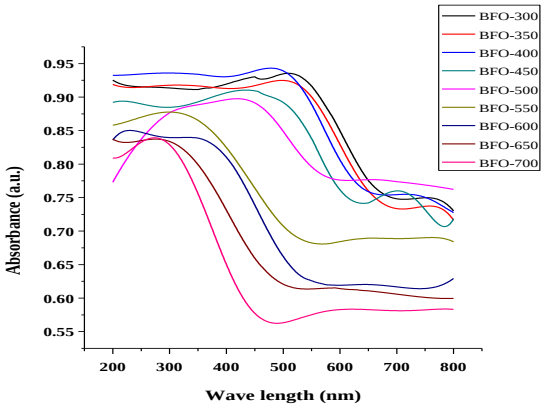

Figure 1(a). UV – Visible spectra of BFO nanoparticles at different annealing temperatures

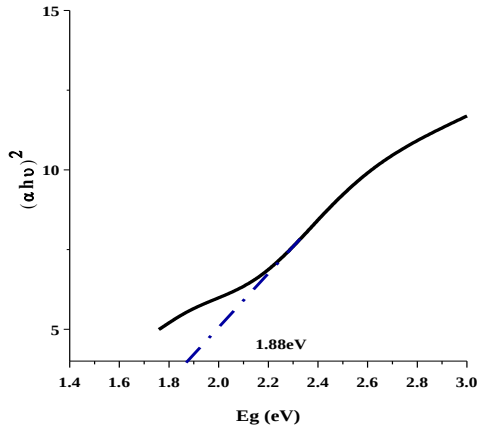

Figure 1(b). Tauc's plot of BFO annealed at 400°C.

The band gap energy of BFO – 400 sample has been calculated from UV – Visible absorption spectrum by plotting a tangent to the spectrum and is found to be 1.84 eV. The absorption of light near band gap for any materials is administrated by the following equation

$$\alpha h\nu = C\,(h\nu - E_g)^n \qquad (1)$$

where α, h, ν, E_g, C and n are absorption coefficient, Planck's constant, frequency of light, band gap and a constant respectively. The corresponding direct band gap energy where n = 2 is calculated according to the equation (1) by plotting the $(\alpha h\nu)^2$ against (hν) and extrapolating the linear portion of $(\alpha h\nu)^2$ to energy (hν) axis at α = 0 and is portrayed in Fig. 1(b). After extrapolation, the band gap energy has been found to be 1.88 eV for BFO–400 nanoparticles and this band gap is quite comparable with the earlier literature [16]. Therefore, the lower band gap of BFO–400 nanoparticles suggests the possible utilization of visible light for photocatalysis.

3. 2. FT – IR spectra

Fig.2 shows the FT–IR spectra of BFO synthesized at various annealing temperature in the range of 300–700°C. At low annealing temperature, there is a band around at 1360 – 1450 cm^{-1} which corresponds to trapped nitrate ions and this peak is not significant at high annealing temperature, i.e., at above 600°C. A band at about 1624 – 1643 cm^{-1} corresponds to the bending vibrations of water [17] and the Bi – O band appeared around at 524–564 cm^{-1}. The band around at 794 – 860 cm^{-1} corresponds to Fe – O stretching and at 420–480 cm^{-1} corresponding to Fe – O bending modes. These peaks confirmed the FeO_6 octahedra in perovskites and indicate the existence of $BiFeO_3$ phase [18].

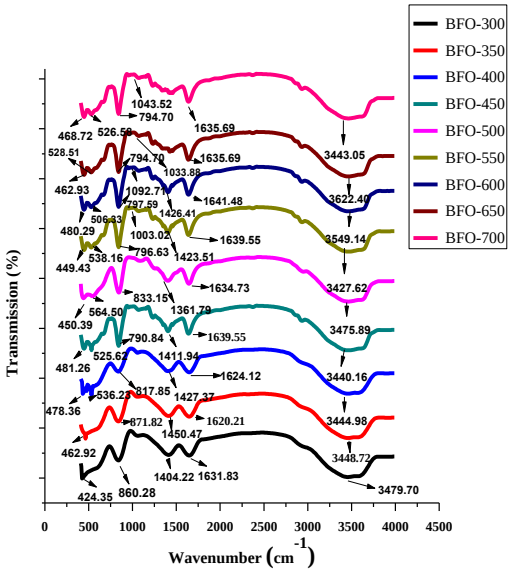

Figure 2. FT – IR spectra of BFO nanoparticles.

3. 3 XRD

From the literature, it is observed that in most of the cases pure BFO and its impurities are formed. David Díaz et al. found that the peak of $Bi_{24}Fe_2O_{39}$ at 2θ = 27.97° and the most intense peak of a by-product $Bi_2Fe_4O_9$ located at 2θ = 28.20° [15]. The formation of such impurities has

also been confirmed by Kothai et al. [19]. Fig. 3 shows the XRD pattern of BFO samples, has the distorted rhombohedral structure of pure bismuth ferrite phase (JCPDS card number 86–1518). The crystalline size was increased with enhanced temperature and the average crystallite size of different samples has been determined from XRD using Scherer's equation. The smallest crystalline size of BFO nanoparticles was found to be 48 nm which is annealed at 400°C. On the other hand, the BFO sample annealed at 700°C produced a large sized particle of 148 nm due to agglomeration and compaction of BFO nanoparticles.

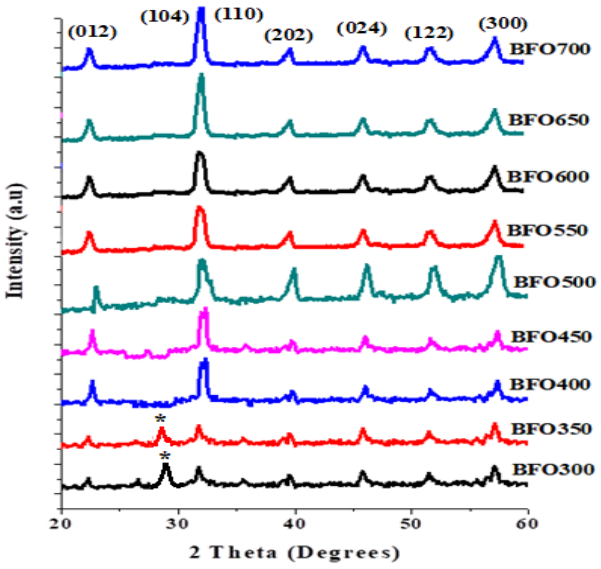

Figure 3. XRD patterns of BFO nanoparticles.

In figure 3, the peaks at 2θ=28.13° and 27.71° for BFO–300 and BFO–350 respectively are due to impurities such as $Bi_2Fe_4O_9$ and $Bi_{24}Fe_2O_{39}$ indicated by asterisk. Also, it has been found that the smaller size of BFO–400 nanoparticles having better photocatalytic activity in comparison with other annealed BFO samples. Table 1 gives the average crystallite size of various BFO samples annealed at different temperatures and the average crystallite size of different samples are plotted against various annealing temperature is as depicted in Figure 4.

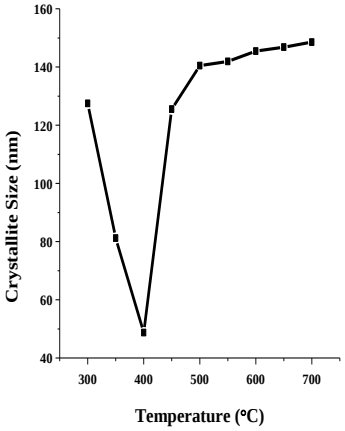

Figure 4. Variation of crystallite size with annealed temperatures.

Table 1: Average crystallite size of bismuth ferrite nanoparticles at different temperatures.

Samples	Size from (012) peak	Size from (104) peak	Size from (300) peak	Average Crystalline size (nm)
BFO–300	127.43	104.70	133.33	121.82
BFO–350	86.15	80.49	79.12	81.92
BFO–400	35.69	61.49	48.78	48.65
BFO–450	120.12	123.08	133.33	125.51
BFO–500	145.45	129.73	146.19	140.46
BFO–550	150	137.14	138.46	141.87
BFO–600	160.18	132.11	144.12	145.47
BFO–650	156.52	126.32	157.54	146.79
BFO–700	163.63	124.14	157.72	148.50

3.4 . SEM analysis

From the literature survey, it has been found that the annealed temperature has an effect on BFO particle size. For instance, the increase in annealing temperature tends the particles to stick together and create larger bodies. BFO thin films annealed at 650°C is denser than the sample annealed at 550°C and 600°C. This is due to the higher crystallinity in the sample annealed at 650°C [20]. Chunlin Fu et al. [21] found that the grain sizes of BFO film annealed at 550°C ranges from 100 nm to 500 nm and the average grain size is 240 nm which is smaller than that annealed at 500°C. It revealed that the average grain

size decreases with increase in annealing temperature, leads to the quantitative increase of single domain grain.

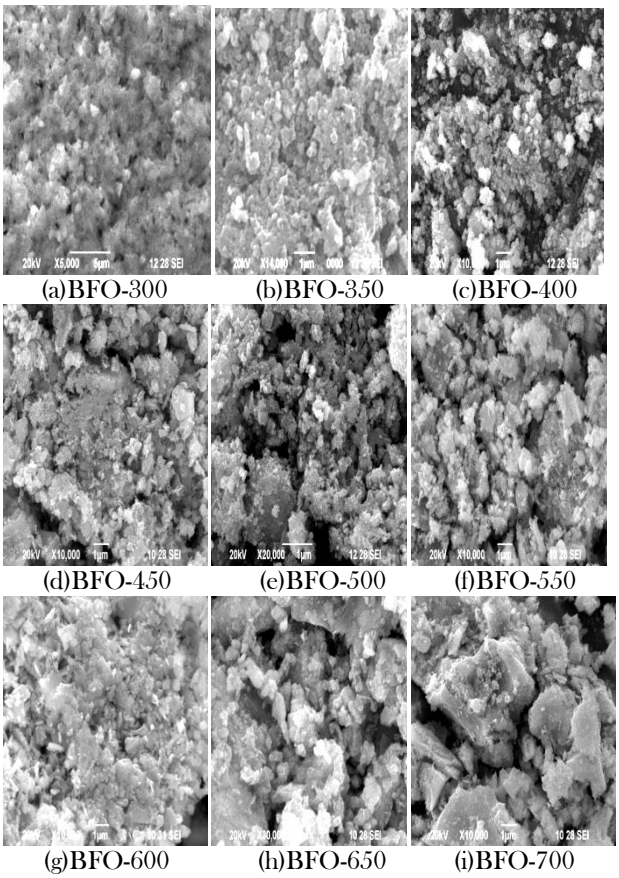

Figure 5. SEM images of BFO at different temperatures.

The SEM images of BFO nanoparticles synthesized at various annealing temperature are shown in Fig. 5. It clearly indicates that the grain size increases with enhanced annealing temperature. The morphology of BFO annealed at 300° and 350°C showed the formation of BFO grains starts and BFO annealed at 400°C showed the spherical shape with more crystallite grain size of 48nm. Further, increase in annealing temperature, increases the grain size of BFO nanoparticles. BFO annealed at 700°C is larger in size in comparison with other annealed BFO samples due to the particles agglomeration and hence larger in size. On the other hand, initially the size of the BFO sample decreased from 300° to 400°C due to formation of single domain grains.

3.5. Photoluminescence studies

Photoluminescence analysis has been used to study the transfer, relocation and recombination process of the charge carriers. The electron – hole recombination rate may be inferred from the intensity of the PL spectrum. An intense PL spectrum indicates a high rate of electron–hole recombination which leads to low photocatalytic activity. It has been observed from the literature, BFO annealed at 800°C exhibits most intense PL peak which has maximum recombination rate of electron – holes and hence exhibit lowest photocatalytic activity. While, the lowest intensity obtained for BFO sample annealed at 500°C is due to the effective transfer of photo – excited electrons through the interface of photocatalyst to the dye solution. Hence, the probability of recombination of charge carrier is minimum in BFO annealed at 500°C with lowest particle size [13]. Also, the presence of secondary phases in BFO may lower the photoluminescence intensity in PL spectrum.

Figure 6 depicts the PL spectra of BFO nanoparticles synthesized at different annealing temperatures. The photoluminescence spectra indicate the visible light emission peak found in the wavelength range of 418–423nm. The intensity of the peaks increases due to the reduction of number of photo generated electron trapped on the surface of BFO, leads to more number of radiative recombinations. The intensity of BFO–400 is lowered due to smaller particle size and minimal recombination of charge carriers and hence results in highest photocatalytic activity. However, the samples BFO –300 and BFO–350 exhibits the low PL signal due to the formation of secondary phases at low annealing temperatures.

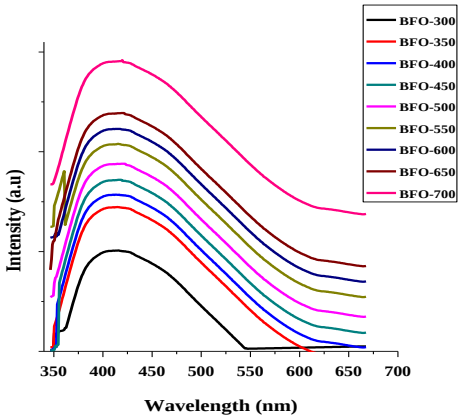

Figure 6. Photoluminescence of BFO nanoparticles

3. 6. Vibrating Sample Magnetometry

The M–H measurements at room temperature have been carried out to study the magnetic behaviour of BFO nano powders. The bulk BFO annealed at 800°C has antiferromagnetic order with magnetization value less than 0.1 emu/g and this low magnetization is owing to the spiral spin structure. Also, a strong size dependent magnetization value and coercivity has been observed. Though the particle size dependent magnetic properties are in good agreement with the literature, the BFO nanoparticles shows the higher saturation magnetization at low applied field. Hence, the magnetization values of the BFO nanoparticles were found to increase significantly with reduction in size [22].

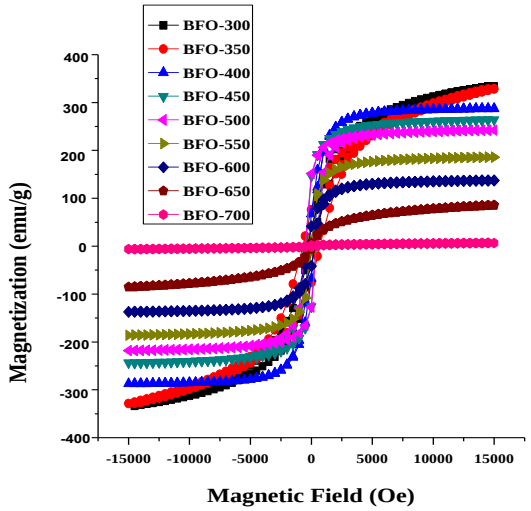

Figure 7. M – H Hysteresis loops of BFO nanoparticles.

Fig. 7 shows the M – H hysteresis of BFO nanoparticles synthesized at different annealing temperatures. The BFO–400 have significant ferromagnetic order at room temperature due to the size less than 62 nm and hence size dependent coercivity. The saturation (M_s) and remanent (M_r) magnetization values are found to be 0.4859 $emug^{-1}$ and 0.3542 $emug^{-1}$ respectively. The samples of BFO annealed at 450–700°C showed the low magnetization, attributed to the spiral spin structure. The incommensurate spin cycloid with wave length of 62 nm leads to the crystal suppressing macroscopic magnetization. Meanwhile, the saturation magnetization (M_s) of BFO–300 and BFO–350 are slightly higher than the other samples, indicating the presence of some undesirable impurity phases [23] which itself shows no contribution to the improved magnetization at room temperature. The coercivity (H_c) values increases with increase in size of BFO nanoparticles and thus BFO annealed at 700°C has higher particle size due to high Hc values. The various magnetic parameters of BFO annealed at different temperatures are given in table 2.

Table 2: The various magnetic parameters of BFO nanoparticles at different annealing temperatures.

BFO (°C)	Hc (Oe)	Ms (emu/g)	Mr (emu/g)
300	61.239	0.4901	0.1313
350	53.281	0.4871	0.0758
400	43.281	0.4859	0.3542
450	63.239	0.4844	0.2862
500	81.107	0.4833	0.2306
550	182.19	0.4743	0.0712
600	255.21	0.4520	0.0639
650	325.26	0.3410	0.0629
700	385.21	0.1188	0.0612

3. 7. Photocatalytic activity

The photocatalytic degradation Rhodamine-B on BFO photocatalyst have been studied at pH = 2.9 by Park et al [24]. This revealed that under visible light irradiation, the absorption peak intensity decreases with increase in time and the absorbance is maximum for the bismuth ferrite with average particle size of 193 nm. Also, a blue shift is observed in the peak position which indicates the formation of intermediate species. If the BFO particle size is downscaled from 193 nm, the photocatalytic efficiency is less.

The influence of pH on the photocatalytic reaction is an important parameter in this study since the photocatalyst is highly dependent on pH as it affects the surface charge of the photocatalyst, degree of ionization and active sites of dye molecules [25]. In this article, the effect of pH has been observed by varying pH of sodium salt of 4-dimethylaminoazobenzene-4-sulfonic acid (methyl orange, MO) dye solution in acidic, neutral and alkaline medium. Methyl orange remains in quinonoid structure and azo form when the pH is below 3.1 and above 4.5 respectively and the photocatalytic degradation rate decreases with increasing pH value. The pH at which the adsorbent surface charge takes a zero value is known as pH of the point of zero charge (pH_{pzc}). The pH_{pzc} of $BiFeO_3$ was found to be 8.0 and at above pH_{pzc} which is alkaline pH the surface of bismuth ferrite is negatively charged and could interact with metal positive species [26]. Hence, higher amount of methyl orange is adsorbed on $BiFeO_3$ when the pH is low in comparison with high concentration of hydrogen ion, due to the positive charge of the catalyst surface which has influence on the anionic dye methyl orange. The increase in degradation rate with decrease in pH of dye solution can also explained by zeta potential of the catalysts.

The photocatalytic degradation efficiency of methyl orange using BFO photocatalyst at different pH of 2, 7 and 10 are shown in Fig. 8. The BFO samples prepared has average particle size of 148.5 nm – 48.65 nm. The degradation percentage of methyl orange with various dose of BFO photocatalyst at pH = 2, 7 and 10 are given in tables 3, 4 and 5 respectively. The sample BFO– 400 has better photocatalytic efficiency under visible light irradiation when the pH=2, because of smaller particle size of 48.65nm. The positively charged surface of the photocatalyst accelerates electron transfer at acidic condition which facilitates the separation of electron-hole pair. The electrons can react with oxygen adsorbed on catalyst surface to generate H_2O_2 which is strong oxidant can completely degrade the methyl orange. While hydroxyl radicals formed in alkaline medium are weak oxidant compared to hole and hence low degradation rate is observed in alkaline condition. The highest degradation efficiency was found to be 96.87% at acidic condition (pH=2) for BFO annealed at 400°C. Thus, the decrease in particle size leads to the quadratic growth of active surface area of the photocatalyst which enhances the photocatalytic activity and also the reduction in the electron–hole pair recombination is responsible for the enhanced photocatalytic activity.

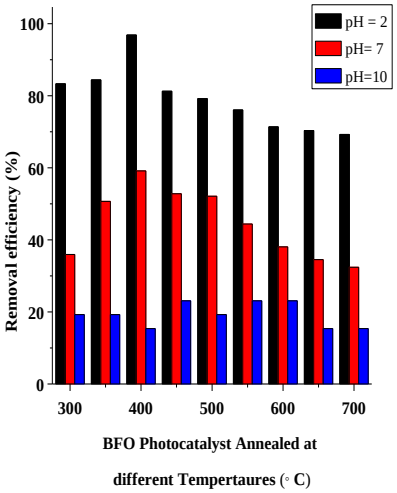

Figure 8. Degradation efficiency of BFO photocatalyst

Table 3: Degradation efficiency of MO at pH=2

BFO (°C)	Dosage of photocatalyst (mgL^{-1})				
	0.1	0.2	0.3	0.4	0.5
300	64.58	66.66	71.87	80.73	83.33
350	52.08	69.27	77.08	81.25	84.38
400	80.21	80.78	81.25	87.50	96.87
450	75.52	77.08	77.60	79.17	81.25
500	69.14	70.88	74.98	76.56	79.17
550	67.71	70.31	72.40	73.96	76.04
600	64.58	66.15	67.71	69.27	71.35
650	63.50	64.58	66.15	68.23	70.31
700	62.50	64.06	65.10	67.71	69.27

Table 4: Degradation efficiency of MO at pH=7

BFO (°C)	Dosage of photocatalyst (mgL^{-1})				
	0.1	0.2	0.3	0.4	0.5
300	16.90	21.83	26.05	33.80	35.92
350	19.01	28.17	30.99	34.51	50.70
400	36.62	41.55	50.70	52.11	59.15
450	26.06	30.99	33.10	38.73	52.81
500	32.39	38.73	49.30	50.70	52.11
550	23.94	33.03	34.51	36.62	44.37
600	15.49	19.01	22.54	26.06	38.03
650	11.97	15.49	16.90	27.46	34.51
700	10.56	13.38	19.01	24.64	32.39

Table 5: Degradation efficiency of MO at pH=10

BFO (°C)	Dosage of photocatalyst (mgL^{-1})				
	0.1	0.2	0.3	0.4	0.5
300	34.62	33.46	23.07	23.07	19.23
350	50	46.15	38.46	30.77	19.23
400	23.08	19.23	15.38	19.23	15.38
450	42.31	34.62	26.92	23.08	23.08
500	38.46	34.62	30.77	23.08	19.23
550	46.15	30.77	30.77	26.92	23.08
600	34.61	30.77	26.92	23.08	23.08
650	34.61	30.77	30.77	19.23	15.38
700	30.77	30.77	23.08	23.08	15.38

4. Conclusion

This research work presents the synthesis of BFO nanoparticles by sol-gel technique at different annealing temperature ranges from 300 to 700°C using ascorbic acid and their structural, magnetic, photoluminescence and photocatalytic analyses has been done. UV-Visible spectral shows the maximum absorption intensity for BFO -400 sample with band gap of 1.88 eV indicates the sample was highly active under solar irradiation. The FT-IR spectra confirmed the formation of BFO nanoparticles from the Bi-O and Fe-O stretching modes. The X-ray diffraction and SEM analyses revealed that increased annealing temperature would increase the size of BFO nanoparticles. Among the samples synthesized, BFO annealed at 400°C appeared to be the best photocatalyst for the de-colorization of methyl orange under solar irradiation owing to the better charge separation and low recombination rate which is also confirmed by PL studies. The VSM studies indicate that the BFO-400 sample has highest magnetization due to its small size (48.65 nm) than spin cycloid wave length of 62 nm. The photocatalytic degradation of methyl orange dye has been carried at different pH of 2, 7 and 10. The high percentage removal efficiency of the MO dye was found to be 96. 87 % at a pH of 2 for the BFO-400 sample.

References

[1] Arnim Henglein, Top. Curr. Chem. 143 (1988) 113–180.
[2] Liqiang Jing, Wei Zhou, Guohui Tian, Hong gang Fu, Chem. Soc. Rev. 42 (2013) 9509-9549.
[3] P. R. Chowdhury, K.G. Bhattacharyya, Dalton Trans. 44 (2015) 6809-6824.
[4] L. Zhang, H. Li, Y. Liu, Z. Tian, B. Yang, Z. Sun, S. Yan, RSC Adv. 4 (2014) 48703 - 48711.
[5] D. Channei, B. Inceesungvorn, N. Wetchakun, S. Ukritnukun, A. Nattestad, J.Chen, S. Phanichphant, Sci. Rep. 4 (2014) 5757.
[6] M. A. Pena, J. L. G. Fierro, Chem. Rev. 101 (2001) 1981-2018.
[7] Y. N. Huo, M. Miao, Y. Zhang, J. Zhu, H.X. Li, Chem. Commun. 47 (2011) 2089 - 2091.
[8] Z. X. Li, Y. Shen, C. Yang, Y.C. Lei, Y.H. Guan, Y.H. Lin, D.B. Liu, C.W. Nan, J. Mater. Chem. A 1 (2013) 823 - 829.
[9] C. M. Cho, J. H. Noh, I. Cho, J. An, K.S. Hong, J. Am. Ceram. Soc. 91 (2008) 3753-3755.
[10] M. A. Ahmeda, N. Okashab, S. F. Mansourc, S. I. El-deka, J. Alloys Compd. 496 (2010) 345–350.
[11] S. Li, Y.H. Lin, B.P. Zhang, Y. Wang, C.W. Nan, J. Phys. Chem. C 114 (2010) 2903-2908.
[12] W.M. Tong, L.P. Li, W.B. Hu, T.J. Yan, G.S. Li, J. Phys. Chem. C 114 (2010) 15298 - 15305.
[13] Sambhu Prasad Pattnaik , Arjun Behera, Satyabadi Martha, Rashmi Acharya, Kulamani Parida, J. Nanopart. Res. 20 (2018) Article 10.

[14] Xiaorui Wang, Chengwei Yang, Ding Zhou, Zhanyong Wang, Minglin Jin, Chem. Phys. Lett. 713 (2018) 185 – 188.
[15] José Luis Ortiz-Quiñonez, David Díaz, Inti Zumeta-Dubé, Humberto Arriola-Santamaría, Israel Betancourt, Patricia Santiago-Jacinto, and Noel Nava-Etzana, Inorg. Chem. 52 (2013) 10306 – 10317.
[16] K. A. McDonnell, N. Wadnerkar, N. J. English, M. Rahman, Denis Dowling, Chem. Phys. Lett. 572 (2013) 78–84.
[17] G.S. Lotey, N.K. Verma, J. Nanopart. Res. 15 (2013) 1553–1566.
[18] G. V. Subba Rao, C. N. R. Rao, J. R. Ferraro, Appl. Spectrosc. 24 (1970) 436 – 445.
[19] V. Kothai, R. Ranjan, Bull. Mater. Sci. 35 (2012) 157 – 161.
[20] ZebinLin, WeiCai, WeihaiJiang, ChunlinFu, ChunLi, YunxiaSong, Ceram. Int. 39 (2013) 8729 – 8736.
[21] Junxiang Hao, Fei Chen, Chunlin Fu, Wei Cai, Yuanyang Sun, Yao Chen, Fengqi Wang, Ferroelectrics 536 (2018) 122–131.
[22] Mehedi Hasan, Md. Fakhrul Islam, Rubayyat Mahbub, Md. Sarowar Hossain, M.A. Hakim, Mater. Res. Bull. 73 (2016) 179 – 186.
[23] Weiwei Hu, Yan Chen, Hongming Yuan, Guanghua Li, Yu Qiao, Yuanyuan Qin, Shouhua Feng, J. Phys. Chem C 115 (2011) 8869 – 8875.
[24] B.P. Reddy, V. Rajendar, M.C. Shekar, S.H. Park, Dig. J. Nanomater. Bios. 13 (2018) 87 – 95.
[25] M. Auta, B. Hameed, Chem. Eng. J. 237 (2014) 352 – 361.
[26] N. Fiol, I. Villaescusa, Environ. Chem. Lett. 7 (2009) 79–84.